Observations on the robustness of internal wave attractors to perturbations

Jeroen Hazewinkel,[1,2,3,a)] Chrysanthi Tsimitri,[4] Leo R. M. Maas,[1,4] and Stuart B. Dalziel[2]
[1]*Royal Netherlands Institute for Sea Research, P.O. Box 59, 1790 AB Texel, The Netherlands*
[2]*Department of Applied Mathematics and Theoretical Physics, University of Cambridge, Wilberforce Road, Cambridge CB3 0WA, United Kingdom*
[3]*Centrum Wiskunde & Informatica, P.O. Box 94079, NL-1090 GB Amsterdam, The Netherlands*
[4]*Institute for Marine and Atmospheric Research Utrecht, University Utrecht, Princetonplein 5, 3584 CC Utrecht, The Netherlands*

(Received 6 November 2009; accepted 28 July 2010; published online 21 October 2010)

Previously, internal wave attractors have been studied in the laboratory in idealized situations. Here, we present a series of experiments in which these conditions are modified. Modifications are made by varying the forcing frequency, by using a nonuniform stratification, by introducing finite amplitude perturbations to the trapezoidal domain, and by using a parabolic domain. All these new experiments reveal the persistence of internal wave attractors that remain reasonably well predictable by means of ray tracing. We conclude that the occurrence of wave attractors is likely to be more general than has previously been thought. The fundamental response of the confined, continuously stratified fluids studied in this paper to a sustained forcing has to be described in terms of internal wave attractors. © *2010 American Institute of Physics*. [doi:10.1063/1.3489008]

I. INTRODUCTION

Stably and continuously stratified fluids support oblique internal wave beams, resulting from a disturbance of the fluid.[1–5] The dispersion relation describing these waves, $\omega = N \cos\theta$, relates the frequency ω to the angle of energy propagation θ relative to the vertical z. The buoyancy frequency $N = \sqrt{-g\rho_*^{-1} d\rho_0/dz}$ is a measure for the background density stratification $\rho_* + \rho_0(z)$, where ρ_* is the average density of the fluid, $\rho_0(z)$ the vertically varying density, and g gravity. The dispersion relation does not depend on the wavelength. In fact, a disturbance with a single frequency normally results in a spectrum of wavelengths.[6] At sloping boundaries, the angle θ is preserved so focusing and defocusing can occur,[7] where the wavelength and amplitude of the reflected wave differ from that of the incident one. In a confined domain, focusing dominates[8] and internal wave attractors (IWAs) can arise. Such IWAs have been observed in the laboratory in a narrow trapezoidal tank, filled with a stable, linearly stratified fluid.[9] The focusing reflection from the sloping wall leads to an energy cascade toward higher wavenumbers,[10] eventually reaching a balance between forcing at the larger scale and dissipation at the viscous scale, observed as a steady state IWA. The clear steady state IWA can be forced by subjecting the fluid to a small horizontal oscillation.[11] The fluid response in terms of an IWA is, theoretically, a fundamental property of almost any periodically forced continuously stratified fluids in an enclosed domain. However, previous observations have been restricted to uniformly stratified fluids in a simple trapezoidal tank with smooth boundaries, lacking any mechanism for scattering of internal waves. Moreover, the forcing frequencies historically used were chosen such that only the simplest of all attractors was found. A natural question then is whether IWAs are also found when perturbations to this simple domain shape or to the linear stratifications are made, or when the forcing frequency is varied.

Studies of reflection of two-dimensional internal wave beams from topography or sharp density jumps have revealed that scattering of the beam structure occurs.[12,13] Given the dispersion relation, a significant part of scattering of internal wave beams from topography consists in fact of focusing and defocusing. This can be easily seen by inviscid ray tracing[14] (the same ray tracing that can be used to find the attractor). For subcritical reflection (beam angle steeper than the angle of the topography) from a sawtooth topography, recent experiments[13] show that there occurs some back-reflection of the waves, defined as the change of sign of both horizontal and vertical wavenumbers. This is not captured by ray tracing, which predicts only forward reflection (the change of sign of only one component of the wavenumber vector[14]). Partial reflection can occur when a wave beam propagates through a changing density gradient.[15,16] In that situation, it is also possible that the internal waves are trapped in parts of the fluid. Given that IWAs consist of multiple reflections and many wave scales, the above effects will play an important role when studying the implication of rough topography or nonuniform density gradients on IWAs.

In this paper we will study the existence of more complicated IWAs in essentially two-dimensional domains and employ ray tracing to predict the shape and location of the IWA.[8] Our starting point is a simple attractor in a fluid, having a constant stratification and smooth side walls, that acts as default experiment to which perturbations will be made. First, we vary the forcing frequency and show that the fluid response with strong internal wave motion depends on the complexity of the IWA that can be formed. Second, we use a nonuniform stratification and show that the attractor now consists of curved rays, albeit reached only after going

[a)]Present address: Scripps Institute of Oceanography, University of California San Diego. Electronic mail: jhazewinkel@ucsd.edu.

TABLE I. Parameters for experiments.

Fixed parameters			
	Length	L	453 mm
	Width	W	120 mm
	Angle of sloping wall	α	0.47 rad
Default experiment			
	Fluid height	H	260 mm
	Stratification	N	2.5 ± 0.1 rad s^{-1}
	Forcing frequency	ω	$2\pi/5.0$ rad s^{-1}
Frequency scan			
	Fluid height	H	300 mm
	Stratification	N	2.2 ± 0.1 rad s^{-1}
	Forcing frequency	ω	
I			$2\pi/5.1$ rad s^{-1}
II			$2\pi/4.8$ rad s^{-1}
III			$2\pi/4.3$ rad s^{-1}
IV			$2\pi/3.9$ rad s^{-1}
V			$2\pi/3.7$ rad s^{-1}
VI			$2\pi/3.5$ rad s^{-1}
Nonuniform stratification			
	Fluid height	H	290 mm
	Perturbation height	h	50 mm
	Stratification basic	N_0	1.8 ± 0.1 rad s^{-1}
	Stratification perturbation	N_1	2.1 ± 0.1 rad s^{-1}
	Forcing frequency	ω	
NU-I			$2\pi/4.5$ rad s^{-1}
NU-II			$2\pi/4.7$ rad s^{-1}
NU-III			$2\pi/4.9$ rad s^{-1}
Corrugated wall			
	Fluid height	H	260 mm
	Stratification	N	2.5 ± 0.1 rad s^{-1}
	Forcing frequency	ω	$2\pi/5.0$ rad s^{-1}
	Corrugation wall	Peak angle (degrees)	nr peaks
P-II		45	20
P-III		45	7
P-IV		45	3

through an interesting transient phase. Then, we perturb one of the side walls with a variety of regular corrugations and find that the small scale focusing from these corrugations complicates the attractor shape but does not suppress the attractor. Finally, we show that attractors, as predicted by ray tracing,[8] also arise in a parabolic domain.

II. EXPERIMENTAL SET-UP

In the idealized laboratory set-up, we use a narrow tank with a single sloping wall, making an angle α with the vertical. The tank has dimensions $L\times W\times H$, see Table I, and is the one also used by Refs. 10 and 17. We fill this tank using two computer-controlled peristaltic pumps feeding in fluids of different densities to produce the desired stable stratification. In this study we use both a linear density stratification and a stratification that is characterized by a steeper gradient in the middle. For the final experiment we use a parabolic channel of width W and filled with a linearly stratified fluid of height H.

TABLE II. Parameters for experiment in parabolic channel.

Parabolic channel		
Fluid height	H	260 mm
Width	W	120 mm
Half length at surface	R	280 mm
Stratification	N	2.5 ± 0.1 rad s^{-1}
Forcing frequency	ω	$2\pi/5$ rad s^{-1}

To measure the motions of the fluid in the tank, we use synthetic schlieren,[18] employing a fixed dot pattern on a light-bank 0.5 m behind the tank. When viewed through the tank, any change in density gradient $\nabla\rho'(x,z,t)$ in the fluid results in apparent movement of the dots due to changes in the refractive index. Synthetic schlieren relies on the correlation of these apparent displacements of the dots and compares them to an unperturbed image. The data are analyzed with the DIGIFLOW software (Dalziel Research Partners, Cambridge). We use a density probe that can traverse through the tank to measure the unperturbed stratification and hence N. The internal waves are forced by horizontally oscillating a platform supporting the tank with an amplitude of 0.03 m at an adjustable frequency. We phase lock the camera with the oscillation, capturing 16 frames evenly spaced through each forcing period. This enables us to perform synthetic schlieren during the steady state of the experiment, with each of the 16 snapshots having its own reference frame. We will present the phase and amplitude of the directly observed horizontal component of the perturbation buoyancy gradient $b_x=-g\rho_*^{-1}\partial\rho'/\partial x$ as this is one component of the directly observed density gradient field.[18] Analysis of b_z and integrated b fields reveals identical behavior[17] and will not be presented. The vertical component does not reveal different dynamics in any of the experiments. We run the experiments for 50 oscillation periods and present most of the data after harmonic analysis (HA) at the forcing frequency from the last 20 periods in the steady state. Harmonic analysis is done by projecting the observations onto a field that oscillates at the forcing frequency, thus reducing the time series to an amplitude field and a phase field. In all experiments we find that the forcing frequency is the only significant frequency when the fluid reaches steady state. All experiments reach steady state in about 20–25 oscillation periods. The experiment in the parabolic channel is presented upon HA at the forcing frequency of the first period after we stopped the forcing (120 snapshots per period). Experimental parameters for this experiment are found in Table II.

For the experiments with the corrugated side walls we had 90° "sawtooth" corrugations of varying length scale, with parameters given in Table I. The corrugations were put onto the vertical side wall of the tank. After placement of the wall in the emptied tank, the tank was refilled with a linear stratification.

III. RESULTS

A. Default experiment

For a fluid with a linear density stratification, N is constant. This means that for a given forcing frequency the wave angle θ is fixed. Therefore, in an enclosed two-dimensional domain, the path followed by internal waves and their reflections can be found by means of a simple iterative procedure. For smooth walls, analytic expressions can be found coupling subsequent reflection points at the walls.[8,19] However, such expressions become unwieldy and unnecessary when complicated domain shapes are considered, such as domains with sawtooth side walls. The iterative procedure, however, can be simply described for constant N. Start with a point at the surface of the tank and "shoot" a ray into the domain at angle θ to the vertical. Find the location of intersection with the wall. The direction that the reflected wave takes is along the only other ray inside the fluid domain that passes through that point at an angle θ to the vertical. If, at the reflection point, the wall is steeper than the ray, then the vertical direction of propagation is maintained. If the wall is less steep, then the direction of vertical propagation is reversed. This determines the new direction of the ray and the procedure is repeated at the next reflection. The rays are followed for 1000 iterations, creating webs. An example is given in Fig. 1(a), where the rays are followed from two points at the surface, the squares colored red and blue. Both the red and blue webs converge to the black trapezoid, the IWA. In fact, all rays from all points in the domain will approach the IWA and, independent of the original direction, will do so in a clockwise direction.[8]

Figures 1(b) and 1(c) demonstrate that this attractor is indeed found in our default experiment and is very similar to the one described in Refs. 10 and 17. From the very gentle sloshing of the fluid in the tank, large scale internal waves are seen to focus onto the attractor. The focusing continues until the smallest wavelengths reach the viscous scale. The width of the beams is determined by a peak in the wavenumber spectrum. This process takes about 25 periods and has been described and explained in detail by Ref. 10. After its initial establishment, the attractor is in steady state. The observations from the last 20 oscillation periods in this steady state, sampling 16 frames per period, are presented after HA in amplitude [Fig. 1(b)] and phase [Fig. 1(c)] plots. The shearing nature of the motion in the beams and the cross-beam phase propagation become visible by the rapid change in phase across the beams, identical to theoretical descriptions of internal wave beams.[6] Phase propagation is directed in the positive direction, such that the phase in the upper-left beam of the IWA propagates downward to the right. Recalling that internal wave energy propagates perpendicular to its phase, such that their horizontal components are aligned and their vertical components opposite, phase propagation is consistent with a clockwise energy propagation around the IWA. The amplitude plot shows the usual decay of the wave amplitude in the beams due to viscous attenuation as we follow the attractor in the clockwise direction, starting from the sloping wall.[10]

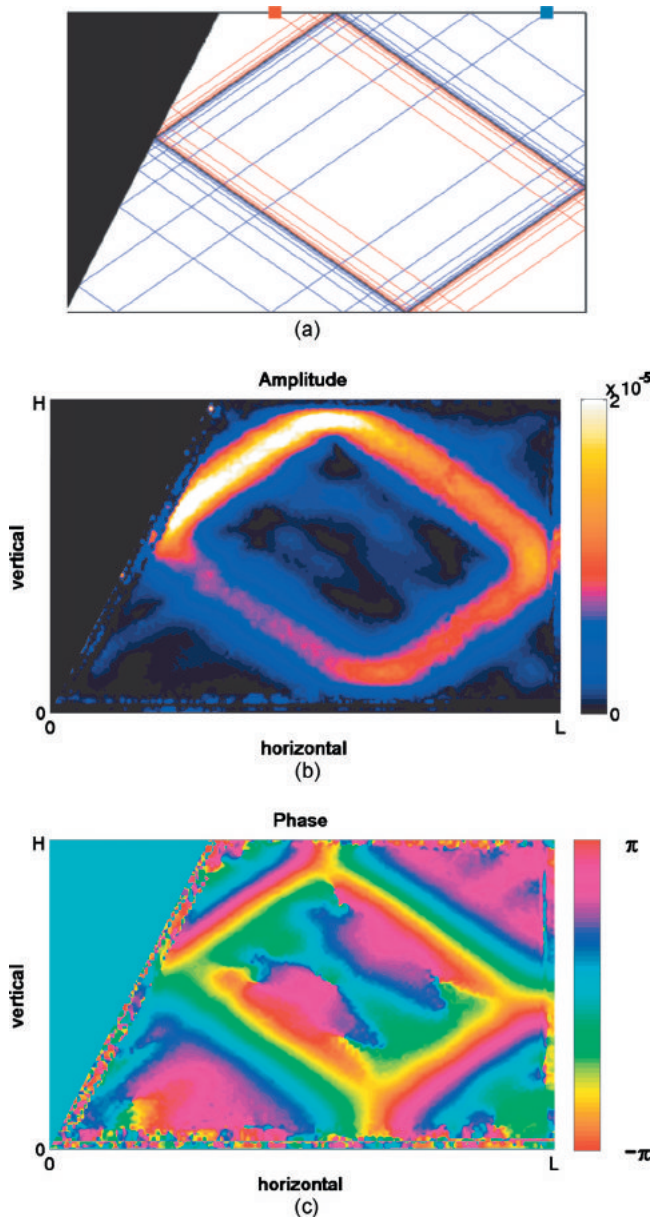

FIG. 1. (Color) Example of ray tracing for the default parameter values. Harmonic amplitude (s^{-2}) and phase (propagation in time from negative to positive) from observations of b_x. Axes and definition of colors will be the same in the following plots.

B. Frequency scan

We vary the frequency in the series of experiments indicated in Table I. The experiments are performed one after another, with sufficient time between experiments to allow the waves to dissipate. By varying the wave angle, i.e., frequency, in the ray tracing we find various attractors. The resulting IWAs are shown in the left-hand column of Fig. 2. These comprise only rays that have converged at the scale of the line thickness. Clearly, when the frequency changes the IWA shape changes, and the experiments reveal clear differences in response of the fluid depending on the forcing frequency. Over continuous frequency intervals, the number of boundary reflections is fixed and, when the number of reflections is small, the IWA has a relatively simple shape. We will denote these simple IWAs by the number of reflections at the

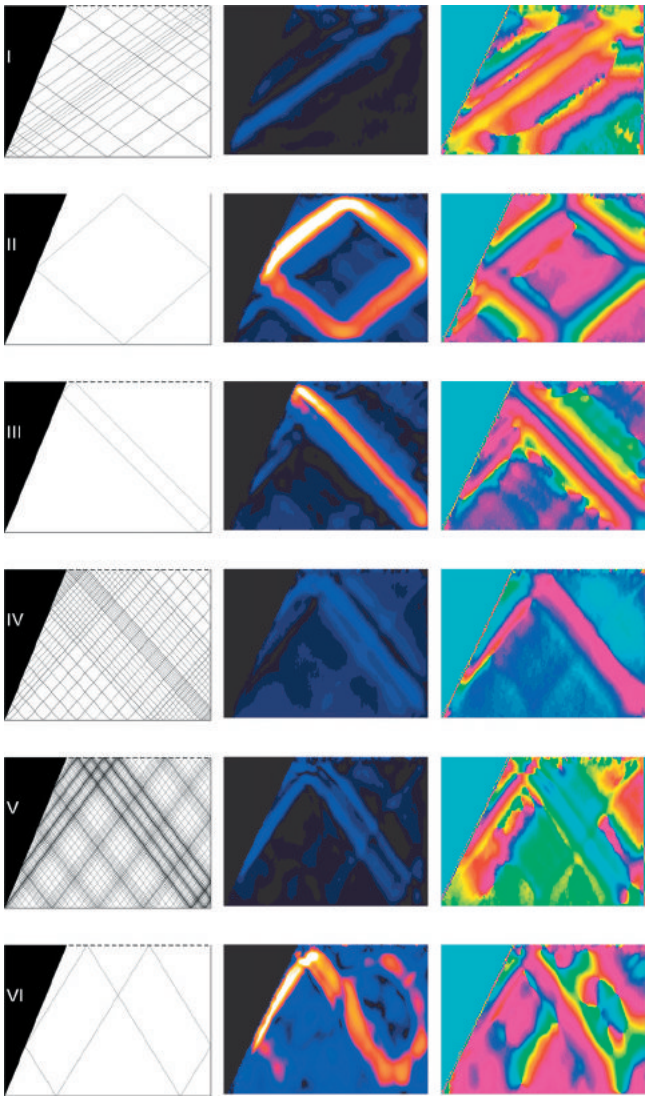

FIG. 2. (Color) IWA spatial structure predicted by ray tracing for varying forcing frequency (left panel). Observations of the observed steady state patterns in terms of harmonic amplitude (middle panel) and phase (right panel). Labels I–VI in the ray tracing plots refer to experimental condition in Table I. For color and axes properties, see Fig. 1.

top and at the vertical side wall, respectively. This means that the IWA in the example of Fig. 1 is a 1-1 IWA while the one at the bottom of Fig. 2 is a 2-1 IWA.

The central column of Fig. 2 shows the amplitude of the corresponding experimental IWA, while the right-hand column shows the phase. The color scheme for these two columns is identical to that used in Fig. 1. The first experiment (I) has a frequency that corresponds to a frequency a bit below the value of the boundary of the frequency interval for a 1-1 IWA. Ray tracing does not suggest a simple structure. Note that although it seems that the rays end in a corner, this is not the case, there are two rays very close to each other. The attractor is really a closed orbit, this will also be the case for the other experiments. Although the response of the fluid is much less pronounced than that of the default IWA, HA still reveals a weak signal. This signal does have a clear phase signature that reflects aspects of the ray tracing. During the next two experiments (II and III), the frequencies are in the 1-1 attractor interval and show a clear amplitude and phase structure comparable to the ray tracing. In the subsequent frequency regimes (IV and V), we find very complex attractors that consist of many loops through the domain. The experiments reveal a weaker response of the fluid. Note, however, that the amplitude and phase again bear traces of the structure from the ray tracing, especially near local zones of denser structure of the IWA. In the 2-1 attractor frequency domain (VI), we find again a clear response of the fluid.

C. Nonuniform stratification

The tank is filled with a fluid characterized by a region of higher N toward the center of the tank. The measured profiles of the density and stratification $N(z)$ are shown in dots to the right of Fig. 3. We approximate this stratification by $N^2(z)=N_0^2+N_1^2\,\mathrm{sech}^2[(z-H/2)/h]$, the solid lines in the figure, that we will use for the ray tracing. This model stratification allows us to exactly compute the rays, see the Appendix for details and Table I for characteristic parameters. The ray tracing shows that this idealized nonuniform ray tracing leads to unique IWAs too, see right of Fig. 3. We perform three experiments with different forcing frequencies, varied in the 1-1 attractor frequency interval.

It is worth describing how the fluid reaches a steady state wave field in these nonuniform stratifications. When the oscillation starts, we observe a strong response in the middle of the tank, with beams that reflect within this more strongly stratified region, reminiscent of wave beam trapping.[15] Initially, internal waves radiating from the sloping side wall have length scales comparable to h, the height of the strongly stratified middle of the stratification. For these larger scale waves, the region is only partially transmissive;[16] scattering takes place. This is not covered by standard geometrical ray tracing which invokes Wentzel–Kramers–Brillouin (WKB) theory,[20] also known as the Liouville–Green method. However, within about three periods of oscillation, wave beams are seen in the whole tank with reflections reaching the sloping wall again. Once the waves get focused their length scale decreases so that the transmissivity of the middle region becomes larger and WKB theory becomes more applicable. From that moment on, the focusing toward the attractor proceeds and reaches steady state after about 25 periods.

The patterns of the waves found in the steady state are easily identified as an IWA, especially in the phase of the HA in Fig. 3. Due to the varying stratification, the wave beams are curved and compare well with the ray tracing. Faint patterns in the background give the impression that there is another attractor visible that we do not find from ray tracing for the given stratifications. Given the phase and thus direction of energy propagation in these beams, we conclude that partial reflection from the strongly stratified region is the source of these structures.

D. Corrugated wall

To understand ray tracing for a domain with a sawtooth side wall, we start with the smooth side wall and 1-1 attractor. Then we vary the number of peaks on the right-hand-side wall, see left-hand column of Fig. 4 and Table I. For these

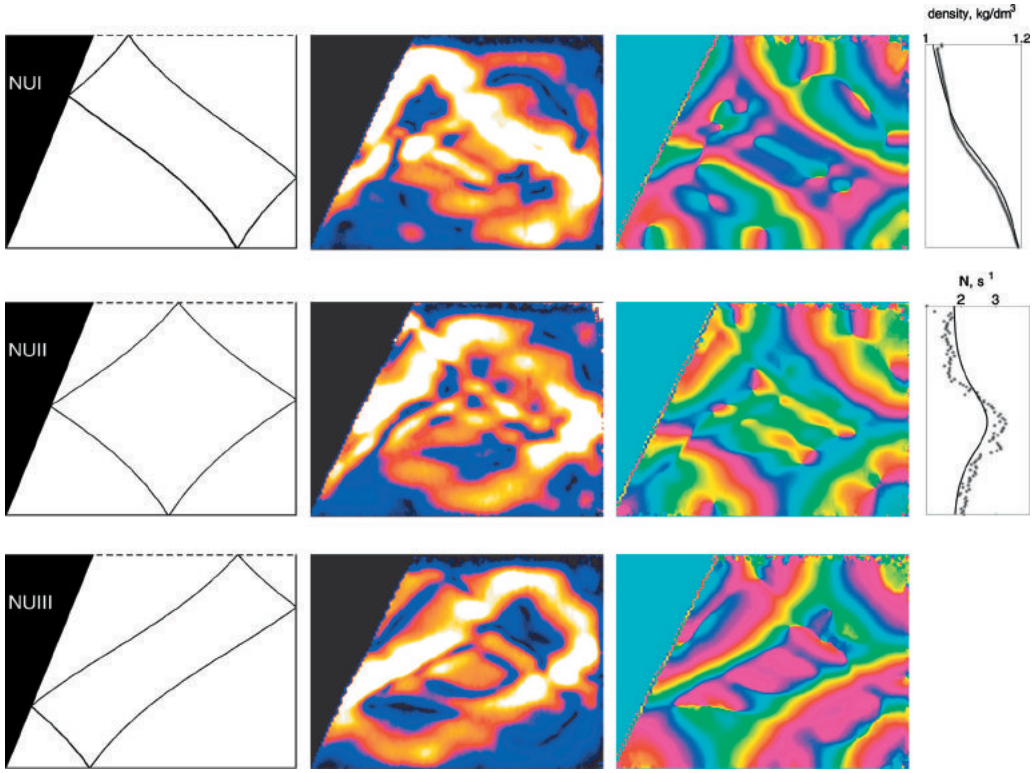

FIG. 3. (Color) As in Fig. 2, but for experiments with nonuniform stratification, for three different frequencies in the 1-1 attractor window. On the right, the measured density profile and $N(z)$, the lines show the approximation used for the ray tracing.

domains, the focusing of internal wave energy takes place at both the sloping wall as well as at the corrugations. The wave focusing of the corrugated side wall is visualized by plotting an incoming bundle of rays, the blue lines, that is focused after reflection, the red lines. For the ray tracing of experiment PII, the black box shows the region in the zoomed view below. In this zoom, we can see that the topography is such that all rays are reflected forward in the ray tracings (i.e., downward to the domain). Continuing the ray tracing leads to attractors very similar to the ones found in the domains without perturbation on the side wall, shown by the black lines in Fig. 4. It turns out that due to the corrugations the original IWA splits into two. In fact, there is a third attractor (not shown) with energy propagation in the defocusing (counterclockwise) direction of the sloping wall. However, the effect of the sloping wall is that most of the rays end up in the focusing direction of the sloping wall and that the focusing power in the counterclockwise direction is significantly less. The third counterclockwise IWA exists due to the combination of a defocusing reflection at the sloping wall at the left and a stronger focusing reflection at the corrugations. The position of this third attractor is between the two attractors in the focusing direction. The positions of the attractors are determined by domain and frequency as before, the small change in domain size due to the presence of the corrugations is of minor importance. The separation is due to the peaks that are nearest to the attractor in the unperturbed case. Note that the ray tracing for the corrugated walls in Fig. 4 shows two 1-1 attractors and not a 2-2 attractor.

The experiment PI with the smallest perturbations, the only one having a slightly larger fluid height than the default depth $H_{\mathrm{PI}}=H+40$ mm, reveals an IWA very comparable to the default case. The initial transients coming from the perturbation on the side wall do not influence the IWA build-up. However, there are thin layers of mixed fluid between corrugation peaks that slowly spread out horizontally during the experiment and change the stratification in the very long term. In the relatively short time of the experiment, it seems that the only effect of the perturbation is that the attractor branches are thinner: experimentally the multiple attractors, found by ray tracing, are not distinguishable due to viscous spreading.

In experiment PII the internal wave pattern changes compared to the default experiment. However, the pattern in steady state is still recognized as a pair of distorted IWAs. The focusing of the corrugation visually breaks the beam structure of the branches. This sort of focusing is also seen in the ray tracing for the corrugation, and is very similar with the observations. In both experiments PII and PIII, the reflection at the corrugation is found at those locations where the attractor branch reflects in the unperturbed situation, indicating the importance of the focusing of the sloping wall.

The reflections from the side wall are further investigated using the Hilbert transform (HT) on the HA fields.[21] With the HT we can identify the directional component of the IWA branches and can separate incoming from reflected waves, indicated by the white arrows in Fig. 5(a). From the ray tracing we found that all rays should be reflected forward. However, this was not found in laboratory experiments on subcritical reflections due to boundary layer and nonlinear

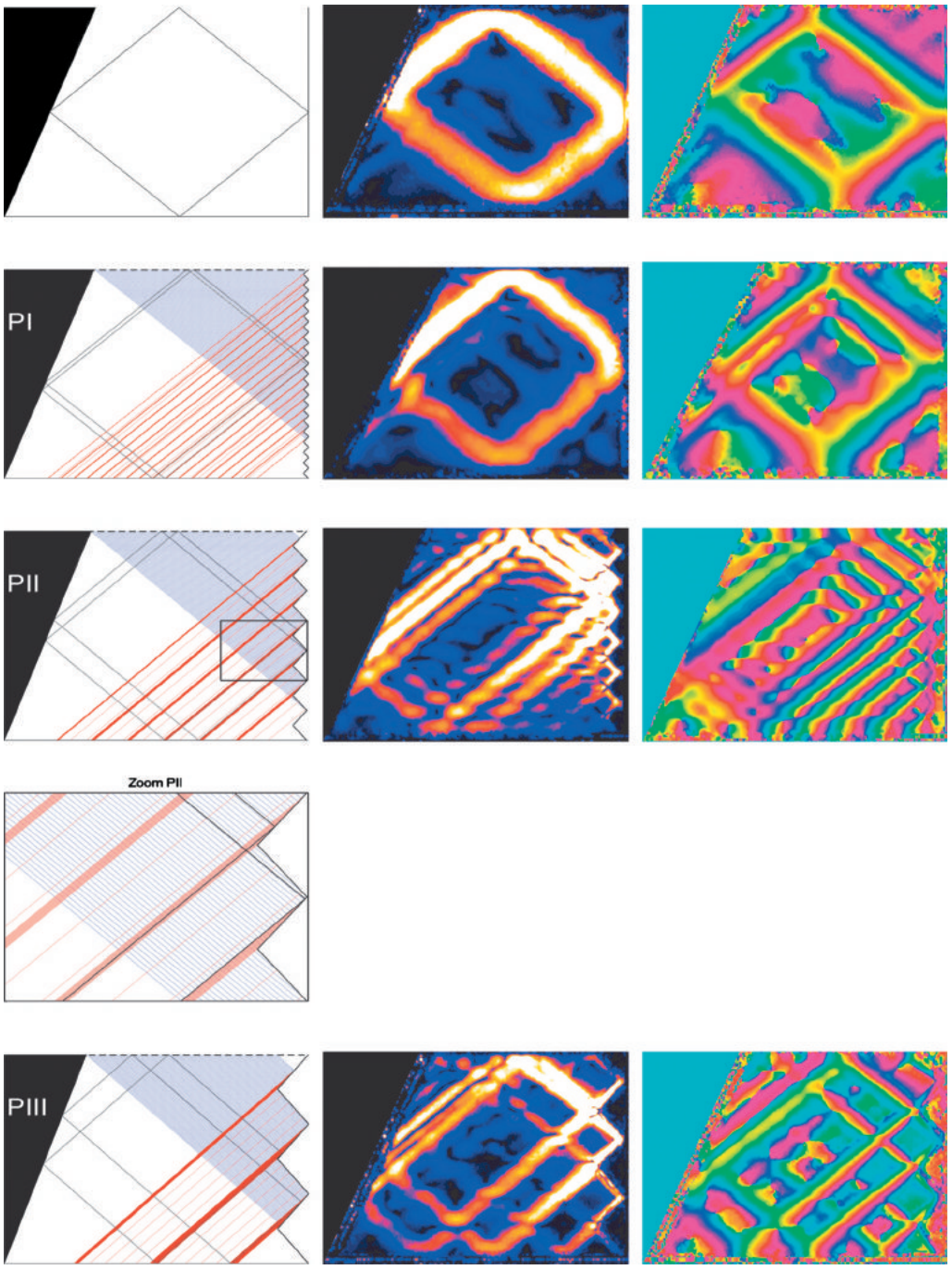

FIG. 4. (Color) As in Fig. 2, but now for experiments with corrugated side wall with decreasing number of corrugations from PI to PIII. Ray tracing for approximations of the experiments showing the breakup of incoming rays (blue lines) by the topography after one reflection (red lines) and subsequent focusing onto the attractors (black lines). Observations of harmonic amplitude and phase resemble these patterns.

processes,[13] and could potentially lead to the formation of the "third" attractor in the counterclockwise direction. Considering the waves in experiment PII, part of the wave energy is indeed back-reflected in the counterclockwise direction, indicated by the ellipses in Fig. 5(a). That these reflections bear the imprint of the corrugations is most clearly seen in the phase plots, see region indicated by ellipses in Fig. 5(b). The imprint is seen in the two upper branches of the attractor, but is not seen after reflection from the slope, which is defocusing in the counterclockwise direction. In the forward (clockwise) reflection, the imprint of the corrugation is clearly seen as a result of the focusing at the corrugations (lower left panels). The dominant direction of propagation remains clockwise.

IV. PARABOLIC CHANNEL

As a last (finite amplitude) perturbation to the domain, we consider a quasi-two-dimensional parabolic channel specified in Table II. For this domain, the ray tracing was investigated in Ref. 8 and numerical studies of the response of a fluid in parabolic domains resulted in attractors, both

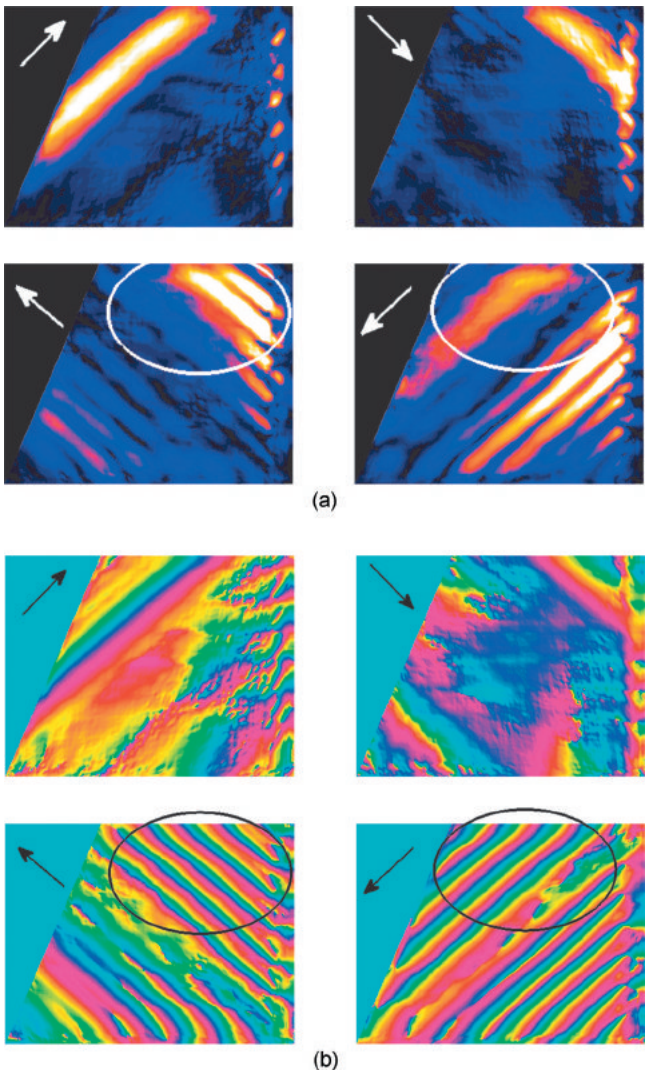

FIG. 5. (Color) Hilbert transform of experiment PII for (a) amplitude and (b) phase, arrows indicate the direction of propagation. Part of the wave energy is back-reflected in the counterclockwise direction, indicated by the ellipses. For color and axis properties, see Fig. 1.

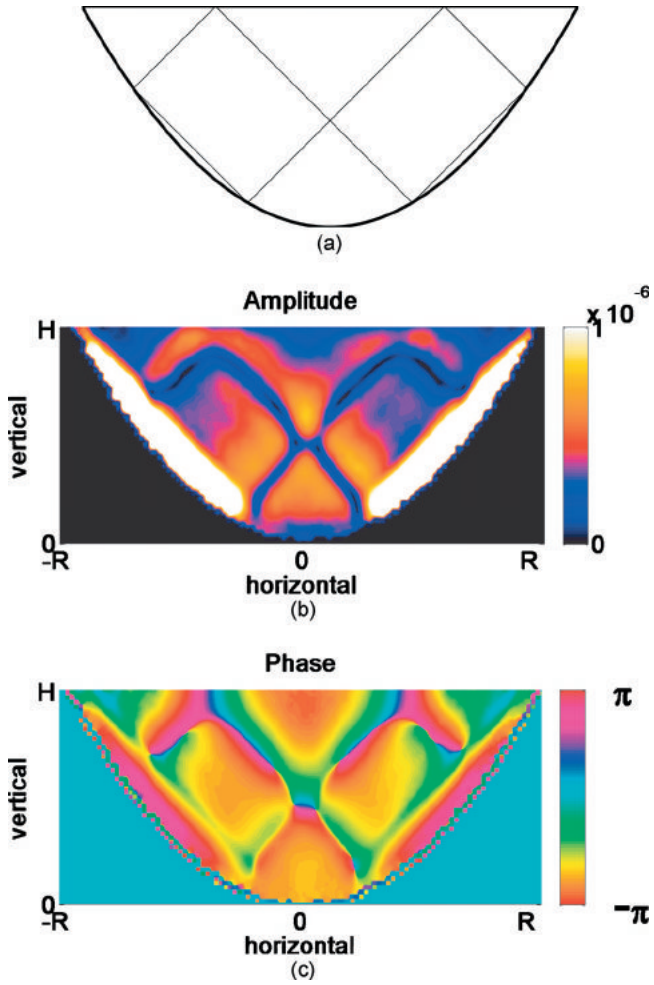

FIG. 6. (Color) (a) Ray tracing, (b) amplitude, and (c) phase for experiment with parabolic channel.

in two-dimensional[22] as well as in three-dimensional channels.[23] We focus on the frequency that leads to the simplest attractor as presented by the ray tracing in Fig. 6(a). This IWA is presented after HA of the initial periods of the unforced decay, where we have a high sampling rate.

We observe a clear IWA structure in both amplitude and phase at the forcing frequency, Figs. 6(b) and 6(c). Since this attractor is a balance between defocusing and focusing, the amplitude of the internal waves, upon focusing reflections high-up at the slopes, is much stronger than the amplitude in the interior. The phase pattern, however, is a clear indication of the continuation of the energy on an IWA.

V. DISCUSSION AND CONCLUSION

In the simple domains in which IWAs have been observed in previous work, ray tracing was always used as a tool to find the attractor location. The present observations have shown that the use of ray tracing in distorted domains can still predict the position of the attractor. Changing the forcing frequency leads to a change in shape of the attractor and sometimes the fluid does not seem to respond to the forcing. However, even when the ray tracing shows a very complicated attractor, we find that some traces remain visible in the phase of the HA.

The values of the parameters used for the ray tracing are representative for the experiments performed. However, especially for situations where the attractors consist of complicated webs, the results from ray tracing are very sensitive to small variations in frequency or stratification. As the largest uncertainties in the observations are in the stratification, indicated in Table I and typically in the order of a few percent, the ray tracing gives an approximate idea of the attractor. Ray tracing can be modified to predict wavenumber spectra,[10] but only for relatively simple attractors where there is good spatial separation between branches. Such modified ray tracing assumes a balance between focusing and viscous dissipation over the length of the attractor. Given the complicated path of the rays for experiments I, IV, and V, it is surprising to find that viscous dissipation is overcome and wave patterns are observed. It is clear that the simpler the attractor, the stronger the internal response of the fluid.

A similar strong internal response of the fluid is observed when a simple attractor can be formed in domains to

which perturbations in stratification or domain shape are made. All IWAs initially grow by the ongoing focusing of large scale waves at the sloping wall starting from the weak sloshing of the water in the whole tank. Most notably, this is of importance when the stratification is nonuniform. In this situation, the large scale waves go through the middle layer and reflect from it. Still, the change in stratification cannot prevent the focusing at the sloping wall and eventually the waves can penetrate through the middle layer and the attractor is formed.

The main effect of the topography can be seen as adding another set of focusing reflections. This means that the transfer to the viscous wavelength takes fewer reflections and input energy is dissipated faster. However, when the size of the topography is close to this viscous scale (experiment P1), the effect on this dissipation is limited. The focusing on larger sized topography is found only at locations where ray tracing predicts the attractor(s). This indicates that the focusing and counterclockwise back-reflections are a result of the IWA formation and not the source of internal wave energy. Spectral analysis, not presented here, indeed reveals that the reflection from the corrugation follows the growth of the waves focused by the sloping wall. More than one attractor is formed, but the topography limits growth both in spectral shape and amplitude.

We conclude that the occurrence of wave attractors is likely to be more general than has previously been thought. The fundamental response of the confined, continuously stratified fluids studied in this paper to a sustained forcing has to be described in terms of internal wave attractors. These attractors are robust. Their appearance does not depend on the geometrical setting being perfect (e.g., nonuniform stratification or domain) as long as the reflectional symmetry of the fluid domain is broken.[24] This conclusion has implications for stratified and the analogous case of rotating fluids in geophysical settings, although the prevalence of attractors in oceans, seas, and lakes remains an unanswered question. While ray tracing may predict the formation of attractors near ridges[25] or even complex attractors involving many reflections in large ocean basins, we do not yet understand how other oceanographic processes such as mean currents and shear may prevent their observation or formation. Relatively simple versions of wave attractors, namely point attractors, have been argued to be of relevance in describing amplification of supercritically reflecting internal tides in stratified canyons[26] and in explaining the ubiquitous spectral peak at the inertial frequency as resulting from trapping of these waves near the intersection of turning surface and bottom at near-critical (inertial) latitudes.[24,27]

The attractor in the parabolic channel bears strong resemblance with the attractor found by a numerical simulation of an internal tide generated in a parabolic channel.[23] It also resembles the streamfunction patterns found by numerical simulations of a lake with a roughly parabolic shape.[28] In terms of the shape of the attractor, the main nondimensional parameter controlling the possibility of detecting an attractor is determined by the combination of aspect ratio and the ratio of wave over buoyancy frequency, such that the shape of the attractor can be determined by ray tracing in a two-dimensional setting. Experiments in fully three-dimensional domains[29] are needed to explore the limitations of this semi-two-dimensional approach.

ACKNOWLEDGMENTS

We thank Pieter van Breevoort for help with experiments that led to an earlier version of the paper. We also thank technicians of the G. K. Batchelor Laboratory (Cambridge) for their help with the experimental set-up. J.H. is supported by a grant from the Dutch National Science Foundation through the NWO/FOM Dynamics of Patterns program.

APPENDIX: RAY TRACING IN NONUNIFORM STRATIFICATION

Ray tracing in a uniform stratification has been used before to predict internal wave patterns.[8] For a depth dependent stratification $N(z)$, ray tracing is still possible as long as the wavelength is much smaller than the scale over which the buoyancy frequency changes.[20,30] The starting point remains the spatial Poincaré equation for the streamfunction

$$[\partial_{xx} - c^2(z)\partial_{zz}]\Psi = 0, \tag{A1}$$

now, neglecting rotation, with $c^2(z) = \omega^2/N(z)^2 - \omega^2$. This is

$$[\partial_x - c(z)\partial_z][\partial_x + c(z)\partial_z]\Psi = 0, \tag{A2}$$

assuming that $cc_z\Psi_z$ is much smaller than $c^2\Psi_{zz}$. This assumption in fact demands that the wave scale is smaller than the typical length scale over which the stratification changes, a small wave or WKB limit. The characteristics (rays) are curved lines along which $\Psi = \text{const}$, defined by

$$[\partial_x \pm c(z)\partial_z]\Psi = 0 \equiv \frac{d}{dx}\Psi[x, z(x)], \tag{A3}$$

when we interpret the changing stratification as a stretching of the coordinates $dz/dx \equiv \pm c(z)$. When we insert the approximation of our nonuniform stratification, Sec. III C, we find

$$\pm dx = \int \sqrt{\frac{N_0^2}{\omega^2} - 1 + \frac{N_1^2}{\omega^2}\operatorname{sech}^2\left(\frac{z - H/2}{h}\right)}\, dz. \tag{A4}$$

By introducing $z = H/2 + hz'$ and $x = \sqrt{N_0^2/\omega^2 - 1}\, hx'$ we can rewrite this as

$$\pm dx' = \int \sqrt{1 + n^2 \operatorname{sech}^2(z')}\, dz', \tag{A5}$$

where $n^2 = N_1^2/(N_0^2 - \omega^2)$. This can be integrated to find the characteristics

$$\pm x' + \xi = n \arctan\left(\frac{n \sinh(z')}{\sqrt{n^2 + \cosh^2(z')}}\right) + \operatorname{arcsinh}\left(\frac{\sinh(z')}{\sqrt{n^2 + 1}}\right). \tag{A6}$$

These characteristics, labeled by integration constant ξ, describe the curved rays and the ray tracing procedure is straightforward. Starting from a point at the boundary, only

two possible directions remain, the inward going ones. Choosing a direction leaves one path, resulting in an iteration similar to the ray tracing for the linear stratification, where subsequent surface positions are calculated.

[1] H. Görtler, "Über eine Schwingungserscheinung in Flüssigkeiten mit stabiler Dichteschichtung," Z. Angew. Math. Mech. **23**, 65 (1943).
[2] L. Gostiaux, T. Dauxois, H. Didelle, J. Sommeria, and S. Viboud, "Quantitative laboratory observations of internal wave reflection on ascending slopes," Phys. Fluids **18**, 056602 (2006).
[3] D. E. Mowbray and B. S. H. Rarity, "A theoretical and experimental investigation of the phase configuration of internal waves of small amplitude in a density stratified liquid," J. Fluid Mech. **28**, 1 (1967).
[4] T. Peacock and A. Tabaei, "Visualization of nonlinear effects in reflecting internal wave beams," Phys. Fluids **17**, 061702 (2005).
[5] B. R. Sutherland, G. O. Hughes, S. B. Dalziel, and P. F. Linden, "Visualization and measurement of internal waves by 'synthetic schlieren'. Part 1. Vertically oscillating cylinder," J. Fluid Mech. **390**, 93 (1999).
[6] N. H. Thomas and T. N. Stevenson, "A similarity solution for viscous internal waves," J. Fluid Mech. **54**, 495 (1972).
[7] T. Dauxois and W. R. Young, "Near critical reflection of internal waves," J. Fluid Mech. **390**, 271 (1999).
[8] L. R. M. Maas and F.-P. A. Lam, "Geometric focusing of internal waves," J. Fluid Mech. **300**, 1 (1995).
[9] L. R. M. Maas, D. Benielli, J. Sommeria, and F.-P. A. Lam, "Observation of an internal wave attractor in a confined stably-stratified fluid," Nature (London) **388**, 557 (1997).
[10] J. Hazewinkel, P. van Breevoort, S. B. Dalziel, and L. R. M. Maas, "Observations on the wavenumber spectrum and decay of an internal wave attractor," J. Fluid Mech. **598**, 373 (2008).
[11] J. Hazewinkel, P. van Breevoort, A. Doelman, L. R. M. Maas, and S. B. Dalziel, "Equilibrium spectrum for internal wave attractor in a trapezoidal basin," in *Proceedings of the Fifth International Symposium on Environmental Hydraulics*, Tempe, AZ, edited by D. Boyer and O. Alexandrova (International Association for Hydraulic Engineering and Research, Madrid, 2007).
[12] T. Gerkema, "Internal and interfacial tides: Beam scattering and local generation of solitary waves," J. Mar. Res. **59**, 227 (2001).
[13] A. Nye, "Scattering of internal gravity waves," Ph.D. thesis, Cambridge University, 2009.
[14] M. S. Longuet-Higgins, "On the reflexion of wave characteristics from rough surfaces," J. Fluid Mech. **37**, 231 (1969).
[15] M. Mathur and T. Peacock, "Internal wave beam propagation in nonuniform stratifications," J. Fluid Mech. **639**, 133 (2009).
[16] J. T. Nault and B. R. Sutherland, "Internal wave transmission in nonuniform flows," Phys. Fluids **19**, 016601 (2007).
[17] J. Hazewinkel, N. Grisouard, and S. B. Dalziel. "Comparison of laboratory and numerically observed scalar fields of an internal wave attractor," Eur. J. Mech. B/Fluids (in press).
[18] S. B. Dalziel, G. O. Hughes, and B. R. Sutherland, "Whole field density measurements by 'synthetic schlieren'," Exp. Fluids **28**, 322 (2000).
[19] L. R. M. Maas, "Wave attractors: Linear yet nonlinear," Int. J. Bifurcation Chaos Appl. Sci. Eng. **15**, 2757 (2005).
[20] J. Lighthill, *Waves in Fluids* (Cambridge University Press, Cambridge, England, 1978).
[21] M. J. Mercier, N. B. Garnier, and T. Dauxois, "Reflection and diffraction of internal waves analyzed with the Hilbert transform," Phys. Fluids **20**, 086601 (2008).
[22] M. Münnich, "On the influence of bottom topography on the vertical structure of internal seiches," Ph.D. thesis, ETH Zürich, 1993.
[23] S. Drijfhout and L. R. M. Maas, "Impact of channel geometry and rotation on the trapping of internal tides," J. Phys. Oceanogr. **37**, 2740 (2007).
[24] L. R. M. Maas, "Wave focusing and ensuing mean flow due to symmetry breaking in rotating fluids," J. Fluid Mech. **437**, 13 (2001).
[25] W. E. Tang and T. Peacock, "Lagrangian coherent structures and internal tide attractors," Chaos **20**, 017508 (2010).
[26] E. T. Petruncio, L. K. Rosenfeld, and J. D. Paduans, "Observations of the internal tide in Monterey Canyon," J. Phys. Oceanogr. **28**, 1873 (1998).
[27] T. Gerkema and V. I. Shira, "Near-inertial waves on the nontraditional beta plane," J. Geophys. Res., [Oceans] **110**, C01003, doi:10.1029/2004JC002519 (2005).
[28] M. Münnich, "The influence of bottom topography on internal seiches in stratified media," Dyn. Atmos. Oceans **23**, 257 (1996).
[29] J. Hazewinkel, L. R. M. Maas, and S. B. Dalziel, "Tomographic reconstruction of internal wave patterns in a paraboloid," Exp. Fluids (in press).
[30] P. G. Baines, "The generation of internal tides by flat-bump topography," Deep-Sea Res. **20**, 179 (1973).